ARTICLE IN PRESS

Next Energy xxx (xxxx) xxx



Contents lists available at ScienceDirect

Next Energy

journal homepage: www.sciencedirect.com/journal/next-energy



A cooperative degradation pathway for organic phenoxazine catholytes in aqueous redox flow batteries

Xiaoting Fang^{a,b,c}, Lifan Zeng^a, Zhiguang Li^{a,b,c,d}, Lily A. Robertson^{c,d}, Ilya A. Shkrob^{c,d,*}, Lu Zhang^{c,d,*}, Xiaoliang Wei^{a,**}

- ^a Indiana University-Purdue University Indianapolis, 425 University Boulevard, Indianapolis, IN 46202, USA
- ^b Purdue University, 585 Purdue Mall, West Lafayette, IN 47907, USA
- ^c Argonne National Laboratory, 9700 South Cass Avenue, Lemont, IL 60439, USA
- ^d Joint Center for Energy Storage Research (JCESR), 9700 South Cass Avenue, Lemont, IL 60439, USA

ARTICLE INFO

Keywords: Aqueous redox flow battery Organic catholyte redoxmer Phenoxazine Decomposition

ABSTRACT

Redox-active organic molecules that store positive charge in aqueous redox flow cells (catholyte redoxmers) frequently exhibit poor chemical stability for reasons that are not entirely understood. While for some catholyte molecules, deprotonation in their charged state is resposible for shortening the lifetime, for well designed molecules that avoid this common fate, it is seldom known what causes their eventual decomposition as it appears to be energetically prohibitive. Here, a highly soluble (1.6 M) phenoxazine molecule with a redox potential of 0.48 V vs. Ag/AgCl has been examined in flow cells. While this molecule has highly reversible redox chemistry, during cycling the capacity fades in a matter of hours. Our analyses suggest a cooperative decomposition pathway involving disproportionation of two charged molecules followed by anion substitution and deprotonation. This example suggests that cooperative reactions can be responsible for unexpectedly low chemical instability in the catholyte redoxmers and that researchers need to be keenly aware of such reactions and methods for their mitigation.

1. Introduction

The recent surge in oil prices stresses the importance of renewable sources of energy. While this is desirable, a more widespread use of these sources is complicated by their intermittency [1,2]. Redox flow batteries (RFBs) can assist in balancing the supply and demand in the electric grid due to their excellent scalability and stable operation [3,4]. Recently, aqueous organic RFBs have attracted great interest. Organic redox-active molecules (known as redoxmers) storing charge in these devices have advantages over other storage materials due to sustainable sourcing, structural diversity, tunable chemical and electrochemical properties, and potentially low material cost [5–7]. Various families of organic redoxmers, including quinones, [8–16] alloxazines, [17,18] viologens, [19–24] phenazines, [25–27] fluorenone, [28] ferrocenes [29–31], nitroxyl radicals [32,33], phenothiazines [34], etc., have been explored as positive (catholyte) or negative (anolyte) materials. Most of these aqueous redoxmers are anolytes; the catholytes have attracted

less attention as there are fewer successes in their development. This is caused mainly by poor stability of their charged states in aqueous medium. For many of the organic catholytes, the instability can be traced to deprotonation of their radical cations [35]. However, even the charged molecules that avoid direct deprotonation can have short lifetime for reasons that are not entirely clear. If there is a common thread for this detrimental behavior, it remains yet unrecognized as in each instance the reaction products are highly specific to the molecules. For example, the oxoammonium cation (charged nitroxyl) undergoes a ring-opening reaction via deprotonation at the β -carbon to the nitrogen atom [33], while charged phenothiazines are oxidized at the sulfur atom [36]. Pursuing mechanistic understanding for general causes of poor stability of the charged molecules is complicated by the reluctance in the community to report underperforming redoxmer candidates. This practice is counter-productive as it slows down materials discovery by reducing it to time- and resource-consuming trial and error. To improve chemical stability of the catholyte molecules, the decomposition

E-mail addresses: shkrob@anl.gov (I.A. Shkrob), luzhang@anl.gov (L. Zhang), xwei18@iupui.edu (X. Wei).

https://doi.org/10.1016/j.nxener.2023.100008

Received 30 December 2022; Received in revised form 11 February 2023; Accepted 14 February 2023

2949-821X/© 2023 The Authors. Published by Elsevier Ltd. This is an open access article under the CC BY-NC-ND license (http://creativecommons.org/licenses/by-nc-nd/4.0/).

Please cite this article as: X. Fang, L. Zeng, Z. Li et al., A cooperative degradation pathway for organic phenoxazine catholytes in aqueous redox flow batteries, Next Energy, https://doi.org/10.1016/j.nxener.2023.100008

^{*} Corresponding authors at: Argonne National Laboratory, 9700 South Cass Avenue, Lemont, IL 60439, USA

^{**} Corresponding author.

pathways need to be understood so that new structures can be designed to avoid the adverse reactions.

The phenothiazines are the case in point. After sulfur oxidation was identified as the catholyte "murder suspect", several groups have sought to improve the chemical stability by replacing the vulnerable sulfur with oxygen. Phenoxazine, consisting of an oxazine fused with two aromatic rings, is the core structure for many natural or synthetic dyes and pharamceuticals [37]. Because of its relatively high redox potential, phenoxazine derivatives have been incorporated in polymer backbones and used as catholyte materials in RFBs and organic radical batteries with high cycling stability in *nonaqueous* electrolytes [38–40]. It was expected that phenoxazine would be stable in aqueous electrolytes, too. Moreover, stability is not the only concern with the redoxmers; good solubility in all states of charge is required to achieve competitive energy density metrics. Recently, a phenoxazine-based dye, Basic Blue 3 (see Fig. S1), with two amino groups in the 3,7-positions, was used as a catholyte in an acidic aqueous RFB [41]. As this molecule has low solubility in water, acetic acid served as a co-solvent to increase the solubility, making the electrolyte excessively viscous and slowing charge transfer reactions at the electrodes. Expensive nitrogen-doped graphene electrocatalysts were necessary to improve cell efficiency. The study highlighted the need to improve solubility of phenoxazine redoxmers without sacrificing the redox kinetics in aqueous electrolytes.

Given these concerns, we have designed a more soluble phenoxazine derivative incorporating a hydrophilic tetraalkylammonium moiety (-NR₄ $^+$). The resulting organic salt, *N*-(3-trimethylammonium-propyl) phenoxazine chloride (NPrPCl), has significantly improved aqueous solubility (~1.6 M) and fast redox kinetics (0.30 cm s $^{-1}$). When it was paired with a viologen analyte in a flow cell, a cell voltage of 1.03 V was obtained. However, to our dismay, we observed rapid capacity fade caused by catholyte degradation. Our work implies vulnerability of the charged phenoxazine to nucleophilic attack by halide anions. Below we argue that this reaction likely proceeds in a concerted fashion involving two charged molecules. While generalizing from a single example is inherently risky, we surmise that such cooperative reactions can be the culprit in other systems, too. Such reactions may be the common thread between the disparate examples of failed systems.

2. Experimental

2.1. Synthesis and characterizations

The synthetic materials, procedures, and characterization of the redoxmers, including *N*-(3-sulfonatopropyl)phenoxazine (SPrP), *N*-(3-trimethylamoniumpropyl)phenoxazine bromide (NPrPBr), *N*-(3-trimethylamoniumpropyl)phenoxazine chloride (NPrPCl), *bis*-(3-trimethylammoniumpropyl)viologen tetrabromide ((NPr)₂VBr₄), and *bis*-(3-trimethylammoniumpropyl)viologen tetrachloride ((NPr)₂VCl₄), are given in Section S1 and Figs. S2 to S9 therein.

Nuclear magnetic resonance (NMR) spectra were obtained using an AVANCE III HD 400 MHz spectrometer (Bruker). The liquid chromatography mass spectra (LC-MS) were obtained using an Agilent 1290 liquid chromatography (LC) - 6545 quadrupole time-of-flight (QTOF) spectrometer under the positive ionization mode. 0.1 wt% Formic acid in water and acetonitrile in gradient were used as the mobile phase. The isotope distributions were computed using ChemDraw Professional. Density functional theory (DFT) calculations were carried out using Gaussian08 suite.

2.2. Electrochemical testing

Cyclic voltammograms (CV) were obtained using a CHI760D potentiostat (CH Instruments). A glassy carbon working electrode, a carbon felt strip counter electrode, and an Ag/AgCl reference electrode (sat. KCl) were used. CV data were recorded for 0.01 M redoxmer in 1 M NaCl for scan rates ranging from 10 to 500 mV s $^{-1}$. Section S2 and Figs.

S15 to S17 therein describe the methods used to estimate the diffusion coefficients (*D*) and the rate constants for electron transfer rate constants at the electrode (k_0) [42].

2.3. Flow cell testing

The cycling stability of NPrPCl was studied in flow cell housed inside a N_2 -filled glove box containing < 1 ppm O_2 . A custom-made flow cell included 2.5-mm thick GFD-type graphite felt electrodes (SGL Carbon) and a 120-µm thick Selemion AMV-N anion exchange membrane (AGC Engineering) with an active area of 5 cm². NPrPCl on the positive side and (NPr)₂VCl₄ on the negative side (at the same molarity) in 1.5 M NaCl were used. The electrolytes were circulated continuously through the cell at a rate of 20 mL min⁻¹ using a Masterflex[®] peristaltic pump. The cells were cycled at a constant rate using a Neware BST 4000 battery tester. To evaluate the cycling stability of NPrPCl catholyte, the (NPr)₂VCl₄ anolyte was used in molar excess. For the 0.05 M test, 15 mL anolyte and 12 mL catholyte were used. For the 0.2 M test, 5 mL anolyte and 3.5 mL catholyte were used. Electrochemical impedance spectroscopy (EIS) was used to estimate the area specific resistance (ASR) of the cell before and after cycling, which was measured with a CHI760D potentiostat (CH Instruments). The ASR was calculated as the product of the high-frequency ohmic resistance (R_{Ω}) with the active area.

2.4. Electron paramagnetic resonance (EPR) spectroscopy

The radical dication of NPrP+ (NPrP2++) was electrochemically generated in an H-cell with an ultra-fine porous ceramic membrane (P5, Adams and Chittenden). Reticulated vitreous carbon electrodes (45 PPI, ERG Aerospace Corporation) and an Ag/AgCl reference electrode were used to control oxidation. 4 mL of 0.02 M NPrPCl in 1 M NaCl was placed in each cell compartment. Under magnetic stirring, the electrolyte was fully charged at a constant current of 4.2 mA. The charging profile is shown in Fig. S14. The purple solution containing the radical dication was placed in a glass capillary, sealed inside a glass EPR tube, and the paramagnetic species was observed using the continuous wave X-band EPR spectroscopy (Bruker ESP300E). The hyperfine coupling constants on ¹H and ¹⁴N nuclei were determined by fitting the firstderivative EPR spectrum numerically (Winsim). To observe the decay kinetics, the EPR spectra were continuously scanned over 100-500 h. Multiexponential fitting of the doubly integrated EPR spectra was used to obtain kinetic time constants.

3. Results and discussion

3.1. Synthesis of NPrPCl

The parent phenoxazine molecule has negligible aqueous solubility and needs to be derivatized for use in aqueous cells. Introduction of ionic groups is one method to increase the solubility [3]. Inspired by the prior work for catholyte redoxmers [43,44], our initial approach was to introduce a sulfonate group into the heterocycle; however, NaSPrP had a unacceptably low aqueous solubility of 0.27 M. Tetraalkylammonium derivatization has been shown to increase solubility of aqueous ferrocene [30], nitroxyl radicals [32], viologen [29], etc. Synthesis of NPrPCl proceeded in two steps with an overall yield of 68 %. Briefly, it involved *N*-alkylation of phenoxazine by (3-bromopropyl)trimethylammonium bromide, followed by anion exchange (Scheme 1a). NPrPCl and NPrPBr have similar aqueous solubility ~1.6 M, which makes them attractive candidate materials for aqueous RFBs.

A Cl⁻-form anion exchange membrane (AMV-N) was used to separate the cell compartments. To minimize possible redoxmer crossover, an established anolyte molecule (NPr)₂VCl₄ that bears two cationic groups was used (Scheme 1b) [29,45] (NPr)₂VCl₄ features a stepwise 2e⁻ redox activity in pH-neutral electrolytes and has a high solubility of 1.86 M in water. To minimize the impact of the possible anolyte decay on the

Scheme 1. Synthetic routes for (a) NPrP and (b) (NPr)₂V.

cycling lifetime and address the catholyte stability, we used only the $1e^{-}$ reduction of this anolyte and provided molar excess relative to the catholyte (Section 2.5).

3.2. Electrochemistry of NPrPCl

A higher redox potential for a catholyte translates into a higher cell voltage and a greater energy density of charged cell fluid. Cyclic voltammetry was used to characterize the redox reactions of NPrPCl in aqueous sodium chloride. As shown in Fig. 1a and S15, NPrPCl has a half-wave potential at 0.48 V vs. Ag/AgCl. The ratio of the oxidation and reduction peak currents is 1.02, suggesting excellent redox reversibility. The second oxidation of NPrPCl is irreversible (Fig. S16). Also included in Fig. 1a is the CV for (NPr)₂VCl₄ anolyte, showing a redox potential of $-0.55\,\text{V}$ vs. Ag/AgCl (see also Fig. S17). Combining the two redoxmers, a cell voltage of 1.03 V is obtained. CV curves for NPrPCl and (NPr)₂VCl₄ at different scan rates were collected, and diffusion coefficients were estimated using Randles-Sevcik analysis (Section S2 and Figs. S15 and S17). Using Nicholson analysis [42], the

electron transfer rate constant for NPrPCl was estimated to be $0.30 \, \mathrm{cm \, s^{-1}}$ (Fig. S15) while $0.39 \, \mathrm{cm \, s^{-1}}$ was obtained for (NPr)₂VCl₄ (Fig. S17). These rate constants are among the highest reported for aqueous redoxmers [46,47].

To evaluate cycling performance of NPrPCl in aqueous flow cells, we first conducted a rate test using voltage-limited galvanostatic cycling (0.6–1.4 V). Figs. S18a and 1b show the voltage profiles and efficiencies, respectively, for a 0.05 M NPrPCl/(NPr)₂VCl₄ flow cell at different current densities. Upon charging, the solutions become intensely colored, the catholyte turning bright crimson and the anolyte turning purple. An average coulombic efficiency (CE) of > 99 % was obtained at all rates. As the current density increases from 10 to 60 mA cm $^{-2}$, the energy efficiency (EE) decreases from 87 % to 57 % due to growing overpotential, while the active materials utilization decreases from 95 % to 50 %. To quantify capacity retention over time, the flow cell was cycled at a constant current density of 10 mA cm $^{-2}$ (Fig. 1c). The average efficiencies were 99 % CE, 89 % VE and 87 % EE, similar to what was obtained in the rate test. Over 200 cycles (\sim 22 h) there was continuous decrease of discharge capacity at a rate of 0.18 %

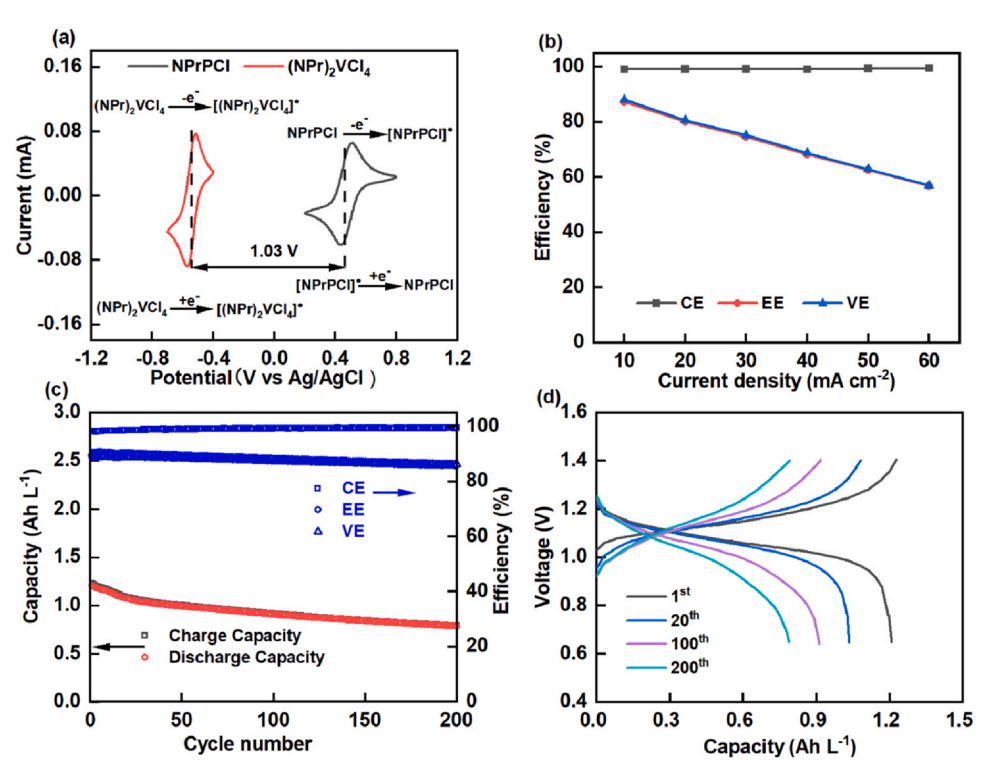


Fig. 1. (a) CV curves of 0.01 M NPrPCl (red) and 0.01 M (NPr)₂VCl₄ (black) in 1 M NaCl obtained (separately) at a scan rate of 100 mV s⁻¹. (b-d) Electrochemical testing of the 0.05 M NPrPCl/(NPr)₂VCl₄ flow cell: (b) CE, VE and EE at different current densities; (c) Galvanostatic cycling at 10 mA cm⁻² showing gradual capacity fade over 200 cycles (22 h). (d) Voltage vs. capacity profiles for selected cycles indicated in the plot. (For interpretation of the references to color in this figure legend, the reader is referred to the web version of this article.)

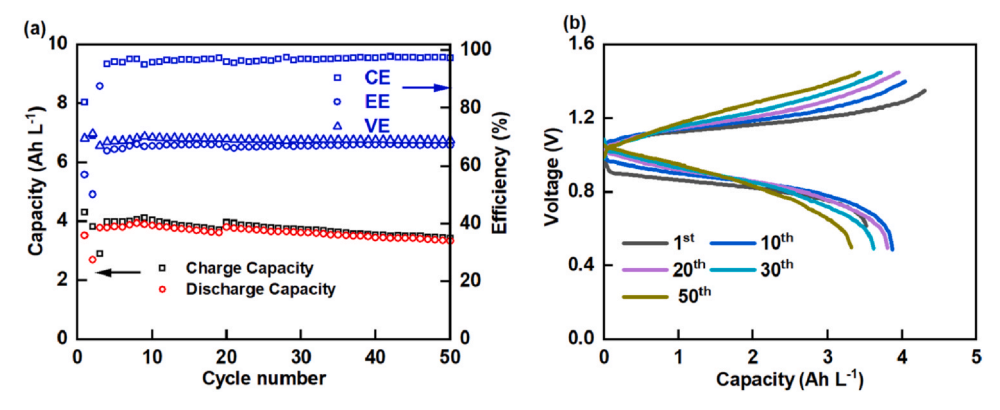


Fig. 2. Cycling data for the $0.2\,M$ NPrPCl/(NPr)₂VCl₄ flow cell: (a) Galvanostatic cycling at $40\,mA\,cm^{-2}$ showing gradual capacity fade over 50 cycles (8 h); (b) Voltage vs. capacity profiles for selected cycles indicated in the plot.

per cycle. Over the same period of time, the ASR remained nearly constant ($\sim 4.6\,\Omega\,\mathrm{cm}^2$), indicating that this loss was not due to increased cell polarization (Figs. S18b and 1d).

To explore the practical limits for energy density, more concentrated electrolytes were tested. For 0.5 M cell (Fig. S19a), the first charge was nearly complete (close to the theoretical estimate of 120.6 mAh), but only 20 % of this capacity was discharged. Thick purple residue separated from the catholyte solution (Fig. S20a) clogging flow lines. The solid material can be redissolved in excess water, so it was from a product with low solubility in electrolyte. To avoid precipitation, the concentrations of redoxmers were decreased to 0.2 M each to obtain more stable cycling. The average efficiencies for this 0.2 M cell were 97 % CE, 69 % VE and 67 % EE (Fig. 2 and S18c). Over 50 cycles (\sim 8 h), the discharge capacity decreased at a rate of 0.16 % per cycle (which is comparable to 0.05 M cell despite a much shorter cycle). Toward the end of this experiment, some precipitation was observed once again, so the cycling was stopped. Clearly, increasing the concentration accelerated capacity fading, suggesting concentration dependent parasitic reactions.

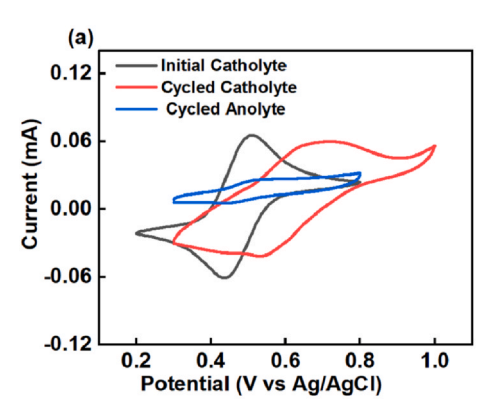
One of the common causes for capacity fading is redoxmer crossover. To determine whether it occurred in our 0.05 M experiment, CV was used to examine the solutions in both compartments before and after cycling. Fig. 3a and b show the voltammograms obtained for the positive and negative sides of the cell across the respective redox regions. This examination indicates that $\sim\!1.6$ % of NPrPCl crossed the membrane from the positive to negative side; i.e., addition of a single charged group did not fully stop the crossover. No crossover or decomposition were observed for the polycation anolyte molecule. Alternatively, use of highly selective membrane such as polymers of intrinsic microporosity (PIM) could mitigate the redoxmer crossover [48]. In the positive side compartment (Fig. 3a), the cycled electrolyte exhibits a half-wave potential that is 180 mV more positive compared to the pristine solution, and two additional redox couples are identified.

This observation suggests advanced decomposition of the active into structurally related species with higher oxidation potentials. For best aqueous redoxmers, the loss of capacity can be as low as 0.001–0.01 % per day [49,50]. Our experiments suggest that degradation of NPrPCl is the likely cause for the observed capacity fade. As the neutral catholyte is very stable, the degradation can only occur in the charged molecule.

3.3. Decomposition of Charged NPrP+

To identify the decomposition products, LC-MS analysis was carried out. A solution containing NPrP^{2+*} was prepared by fully charging a 0.05 M NPrPCl/(NPr)₂VCl₄ flow cell. The catholyte solution was removed from the cell, aged for two weeks, diluted 1:50 v/v with water, and analyzed chromatographically. As shown in Fig. 4a, two major chromatographic peaks were observed. Fig. 4b shows the mass spectrum for the first major peak. The mass peak at m/z 317 can be assigned to a monochlorinated product (NPrP-[Cl]). This attribution is also supported by observing the mass peaks with m/z 230 and 258 for the fragments FGT1 and FGT2, respectively. As chlorine has two naturally abundant isotopes, the chlorination is also seen from the isotope distributions of these mass peaks shown in Fig. 4b and c. In the same fashion, the second chromatographic peak in Fig. 3c is attributed to the dichlorinated product (NPrP-[Cl]₂). Note that these mass spectra do not indicate the site for chlorine substitution. However, previous reports on chemical oxidation of phenoxazines suggest preferential attacks in the C3 and C7 positions in phenoxazine ring [51]. While this preference was observed before our study, it remained unexplained.

From these results, we infer that chlorination of NPrP^{2+*} is the major decomposition pathway, with the chloride in the electrolyte being the source of chlorine. The electron withdrawing by the chlorine groups causes a positive shift in the redox potential of the products, which agrees with the data in Fig. 3a. The co-existence of NPrP-[Cl] and NPrP-[Cl]₂ would account for the observed two redox events in the



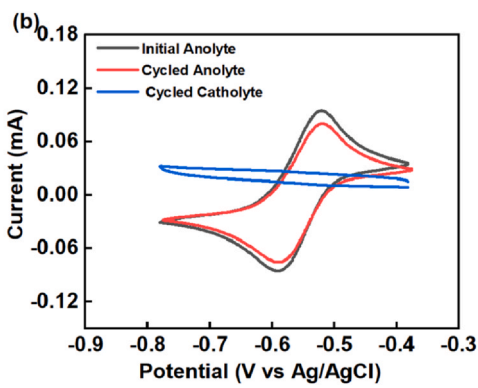


Fig. 3. CV curves in the potential ranges of (a) NPrPCl and (b) $(NPr)_2VCl_4$ before and after cycling of the flow cell in Fig. 1. The scan rate was 100 mVs⁻¹.

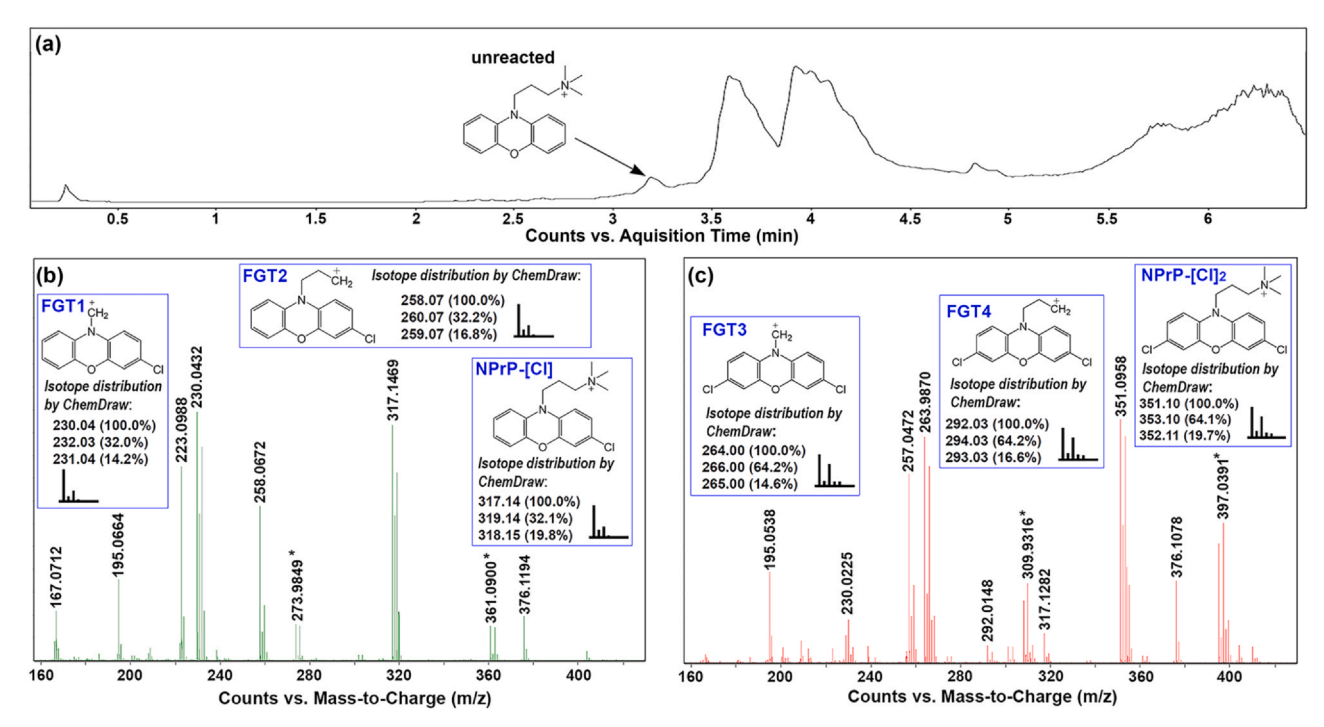


Fig. 4. LC-MS for charged 0.05 M NPrPCl in 1 M NaCl after two-week aging: (a) The total ion current chromatogram; (b) The mass spectrum corresponding to the chromatographic peak at the retention time of 3.47-3.78 min; (c) Ditto for 3.85-4.30 min. The computed isotope signatures are shown along with fragment structures (FGT). (The asterisked m/z peaks arise from the brominated residue due to incomplete ion exchange during synthesis of NPrPCl).

voltammogram of cycled solution. In a previous report, the dimerization products of phenoxazine were observed in acetonitrile [51]. In our LC-MS analyses of aqueous solutions, no dimers were observed.

To confirm this decomposition mechanism, we continued to investigate the cycled catholyte from a flow cell test using the same LC-MS methodology. Using NPrPBr in place of NPrPCl (also at 0.05 M in 1 M NaCl) provides another way to establish the presence of mono- and di- substituted halogenated products. Bromide compounds have characteristic isotope patterns in the mass peaks due to the presence of ⁷⁹Br and ⁸¹Br isotopes (50.7 at% and 49.3 at%) in the ions. After the cycling, the solution was diluted and characterized by LC-MS. The LC-MS results are shown in Fig. S20; also shown are the assignments of the major peaks. Similar products were identified to those for NPrPCl, including monochlorinated (NPrP-[Cl], m/z 317), monobrominated (NPrP-[Br], m/z 361), the mixed chloro- and bromo- substituted NPrP (NPrP-[ClBr], m/z 395), and dibrominated NPrP (NPrP-[Br]₂, m/z 439). Thus, the nucleophilic addition of halide anion is not unique for the chloride.

As the halogenated molecules are the main reaction products, these results suggest that precipitation observed in concentrated charged solutions could be due to accumulation of these products. To test this hypothesis, 3,7-dibromoNPrP (NPrP-[Br] $_2$) was synthesized (Section S1.5 and Figs. S10 to S13). This molecule has deep purple color similar to the precipitate found in the flow cells. The solubility of this compound in water was 0.11 M, but only ~ 1 mM in 1.5 M NaCl, which is much lower compared to NPrPCl. The (di)halogenation decreases aqueous solubility of NPrPCl explaining the formation of solid residue during continuous cycling of concentrated solutions.

Since NPrP²⁺⁺ is an open shell species, EPR spectroscopy can be used to characterize this radical dication and follow its side reactions. The radical dication was freshly prepared by charging 0.02 M NPrPCl in 1 M NaCl in an H-cell. The identity of the species was established by diluting the charged solution to suppress spin exchange and resolve resonance lines. The obtained hyperfine coupling constants on ¹H and ¹⁴N nuclei match well with those calculated by DFT (Fig. S21), confirming its identity as the radical dication. Fig. 5a shows the time progression of the EPR spectra for 0.02 M solution and Fig. 5b shows the evolution of the doubly integrated EPR spectra on the logarithmic

time scale (trace i). This quantifies the decay of all unpaired electrons normalized by their initial concentration. The decay kinetics are bimodal: there is a fast component responsible for 65 % of the decay with the half-life time constant of 18.4 h and a much slower component with the half-life time constant of 750 h accounting for the remaining 35 % of the decay. On this long time scale, the EPR spectrum undergoes a transformation as the spectrum from the radical dication gradually fades and a secondary radical species with a narrow EPR spectrum gradually emerges (Figs. 5a and S22). Since the wings of the NPrP²⁺ spectrum do not overlap with the secondary species, one can computationally decompose the EPR spectra into linear combinations of the contributions from the primary and secondary radicals as shown in Fig. S22. Trace i in Fig. 4b shows the result of this decomposition for the radical dication (trace ii) and the secondary radical (trace iii). The slow formation kinetics for the latter species mirrors the slow decay of the radical dication, so the two species are related. At 500 h, ~6 % of the radical dication is converted to this secondary radical. Given that (1) the time scale for this slow transformation is much longer than the duration of our flow cell experiments and (2) the yield of the secondary radical is quite low, it is unlikely that this transformation interfered with the cycling of flow cells. Therefore, we did not delve into the identity of this secondary radical. In contrast, the time constant for the fast component is commensurate with the duration of the cycling tests and can be responsible for the rapid capacity fade. As this component accounts for most decay of the radical dication, we associate it with the halogenation observed in the product analyses. EPR spectroscopy suggests that this fast component becomes faster at higher concentrations: e.g., at 0.5 M, it was only 1 h (Fig. S23). This suggests that the reaction is concentration dependent. We remind that the same was suggested by our cycling experiments.

The observation of concentration dependent kinetics and specificity for halogenation led us to suggest the reaction mechanism shown in Scheme 2. The key insight of this scheme is that the reaction involves two charged phenoxazine molecules. The radical dications (NPrP²⁺) in solution are in the disproportionation equilibrium with their parent cation (NPrP⁺) and the doubly oxidized trication species (NPrP³⁺). The free energy for this reaction is given by the difference in the redox

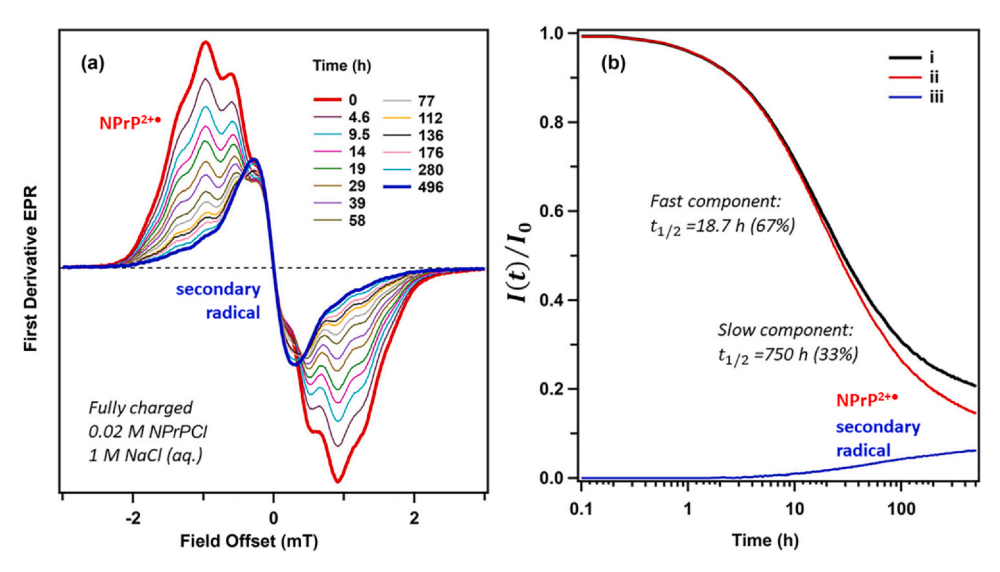


Fig. 5. (a) Time progression of first-derivative EPR spectra from the charged 0.02 M NPrPCl (9.44 GHz, 100 kHz modulation, 0.05 mT modulation amplitude, 300 K). The initial EPR (red) is from NPrP^{2+*}. Over time, NPrP^{2+*} decays and a narrow singlet resonance from a secondary radical appears. (b) Trace i is the ratio $I(t)/I_0$ of doubly integrated EPR spectra normalized by the initial value of this integral plotted on the logarithmic time scale. This quantity represents loss of all unpaired electrons in the system. By estimating the fractions of the two radicals in the EPR spectra, this can be decomposed into the contributions from NPrP^{2+*} and a secondary radical (traces ii and iii, respectively).

Scheme 2. The proposed cooperative decomposition pathway for halide substitution in NPrP^{2+*}.

potentials for 1e and 2e oxidation of NPrPCl, so the reaction strongly favors the direction towards the two radical species. However, as the doubly oxidized molecule is extremely unstable (see Fig. S16), it readily reacts with the halide anion forming the adduct shown in Scheme 2 that promptly loses a proton. This irreversible reaction shifts the equilibrium resulting in a gradual loss of the radical dication and the formation of halogenated product(s). While this reaction can have more complex mechanism than sketched in Scheme 2, it explains the "mystery" of how charged catholytes can deprotonate when direct hydrolytic deprotonation is energetically unfavorable. Indeed, what is prohibitive for an isolated oxidized molecule can still be achieved through their concerted reaction, with the anion providing an agent for nucleophilic attack and the water serving as a proton acceptor. The suggested mechanism readily accounts for the specificity of nucleophile substitution in the C3 and C7 positions of phenoxazine ring that are favored in the adduct shown in Scheme 2.

In this regard, it may be relevant that the radical cations of phenoxazine and phenothiazine readily form $\pi\text{-stacks}$ in the crystals and solutions [52–54]. While their progenitor molecules are bent (so their $\pi\text{-stacking}$ is less efficient), the charged molecules are flat (Fig. S24), and the stacking energy is sufficiently high to overcome electrostatic repulsion of the cores when the charge is screened by anions. While $\pi\text{-stacks}$ form only fleetingly in solution, this stacking boosts cooperative reactions by placing the radical cations into close proximity to one another. As the $\pi\text{-stacks}$ always have a wavefunction admixture of the charge-transfer state, this stacking provides a narrow chemical gate for decomposition of the radical cations. The reaction is particularly fast in aqueous electrolytes due to the high concentration of halide anions and proton accepting by water.

4. Conclusion

In conclusion, through derivatization with a charged N-chain we developed a phenoxazine redoxmer that was highly soluble (1.6 M) in saline solutions without a co-solvent. This molecule has relatively high redox potential and fast redox reactions on carbon electrodes. Unlike the related phenothiazine, it avoids oxidation at the heteroatom. However, the charged molecule still decayed rapidly on the time scale of our cycling experiments resulting in capacity fade. The latter was compounded by permeation through an anion exchange membrane and (in concentrated solutions) product precipitation, but the main cause was the loss of active. Using chromatographic analyses, we established that the catholyte was degraded into mono- and di- halogenated products with the halogen atom supplied by the electrolyte. The substitution in the aromatic ring of the catholyte molecule decreases solubility in electrolyte causing precipitation of the product from the solutions. The spectroscopic study of radical species in charged solutions revealed complex dynamics for the decay of the radical. The concentration dependent fast component of these kinetics accounts for the rapid loss of charged catholyte in our cycling experiments.

On the strength of these observations, we suggest a cooperative charge transfer reaction involving two radical species occurring in concert with nucleophile attack by the halide anion and deprotonation. The reaction could be mediated through the formation of radical π -stacks which are known to occur for phenothiazine derivatives. The recognition for the importance of such reactions is the main import of this study as it suggests a general mechanism in pH-neutral electrolytes through which charged catholytes molecules can evade the design strategies aimed at the stabilization of individual molecules. Perhaps a wide range of

decomposition pathways becomes possible through this cooperation providing the common thread that becomes obscured by the multiplicity of the decomposition pathways. It suggests that chemists need to think beyond the conventional reactions and seek to reverse these cooperative effects.

A possible strategy for suppressing this reaction channel can be by placing multiple charged groups on the heterocyclic cores to increase electrostatic repulsion between the charged states. The same strategy would decrease membrane crossover, largely for the same reason. As such multiple-charge derivatization becomes increasingly popular to reduce membrane crossover [24], the chemists would be delighted to learn that they also inadvertently stabilize their redoxmer molecules by retarding concerted reactions of their charged states. A wider awareness of this connection can be useful in catholyte development.

Author contributions

X.W. and **L.Zhang** conceptualized, designed and directed this work; X.F. performed redoxmer synthesis, electrochemical tests, data analysis, and manuscript drafting; I.A.S. carried out EPR tests, data analysis, and DFT calculations; L.A.R. did electrochemical tests for EPR analysis; L.Zeng did LC-MS characterizations; all authors contributed to manuscript editing.

Declaration of Competing Interest

The authors declare the following financial interests/personal relationships which may be considered as potential competing interests: Xiaoliang Wei reports financial support was provided by National Science Foundation. Lu Zhang reports financial support was provided by US Department of Energy. Xiaoliang Wei reports financial support was provided by Argonne National Laboratory.

Acknowledgements

The authors acknowledge financial supports from National Science Foundation (Award No. CHE-2055222) and from the Joint Center for Energy Storage Research (JCESR), an Energy Innovation Hub funded by the U.S. Department of Energy, Office of Science, and Basic Energy Sciences. This research was also partially supported by Laboratory Directed Research and Development (LDRD) funding from Argonne National Laboratory, provided by the Director, Office of Science, of the U.S. Department of Energy under Contract No. DE-AC02-06CH11357.

Appendix A. Supporting information

Supplementary data associated with this article can be found in the online version at doi:10.1016/j.nxener.2023.100008.

References

- [1] W.A. Braff, J.M. Mueller, J.E. Trancik, Nat. Clim. Change 6 (2016) 964-969.
- [2] B. Obama, Science 355 (2017) 126-129.
- X. Wei, W. Pan, W. Duan, A. Hollas, Z. Yang, B. Li, Z. Nie, J. Liu, D. Reed, W. Wang, ACS Energy Lett. 2 (2017) 2187–2204.
- [4] W. Lee, M. Jung, D. Serhiichuk, C. Noh, G. Gupta, C. Harms, Y. Kwon, D. Henkensmeier, J. Membr. Sci. 591 (2019) 117333.
- B. Huskinson, M.P. Marshak, C. Suh, S. Er, M.R. Gerhardt, C.J. Galvin, X. Chen, a. Aspuru-Guzik, R.G. Gordon, M.J. Aziz, Nature 505 (2014) 195–198.
- [6] V. Singh, S. Kim, J. Kang, H.R. Byon, Nano Res. 12 (2019) 1988-2001.

- [7] X. Fang, Z. Li, Y. Zhao, D. Yue, L. Zhang, X. Wei, ACS Mater. Lett. 4 (2022) 277-306.
- [8] K. Lin, Q. Chen, M.R. Gerhardt, L. Tong, S.B. Kim, L. Eisenach, A.W. Valle, D. Hardee, R.G. Gordon, M.J. Aziz, Science 349 (2015) 1529-1532.
- [9] M.R. Gerhardt, L. Tong, R. Gómez-Bombarelli, Q. Chen, M.P. Marshak, C.J. Galvin, A. Aspuru-Guzik, R.G. Gordon, M.J. Aziz, Adv. Energy Mater. 7 (2017) 1601488.
- [10] Z. Yang, L. Tong, D.P. Tabor, E.S. Beh, M.A. Goulet, D. De Porcellinis, A. Aspuru-Guzik, R.G. Gordon, M.J. Aziz, Adv. Energy Mater. 8 (2018) 1702056.
- [11] M.-A. Goulet, L. Tong, D.A. Pollack, D.P. Tabor, S.A. Odom, A. Aspuru-Guzik, E.E. Kwan, R.G. Gordon, M.J. Aziz, J. Am. Chem. Soc. 141 (2019) 8014-8019.
- [12] Y. Ji, M.A. Goulet, D.A. Pollack, D.G. Kwabi, S. Jin, D. De Porcellinis, E.F. Kerr, R.G. Gordon, M.J. Aziz, Adv. Energy Mater. 9 (2019) 1900039.
- [13] S. Jin, Y. Jing, D.G. Kwabi, Y. Ji, L. Tong, D. De Porcellinis, M.-A. Goulet, D.A. Pollack, R.G. Gordon, M.J. Aziz, ACS Energy Lett. 4 (2019) 1342-1348.
- [14] M. Wu, Y. Jing, A.A. Wong, E.M. Fell, S. Jin, Z. Tang, R.G. Gordon, M.J. Aziz, Chem 6 (2020) 1432–1442.
- [15] G. Park, W. Lee, Y. Kwon, Int. J. Energy Res. 46 (2022) 3362-3375.
- [16] W. Lee, G. Park, Y. Kwon, Chem. Eng. J. 386 (2020) 123985. [17] K. Lin, R. Gómez-Bombarelli, E.S. Beh, L. Tong, Q. Chen, A. Valle, A. Aspuru-Guzik, M.J. Aziz, R.G. Gordon, Nat. Energy 1 (2016) 1-8.
- [18] A. Orita, M.G. Verde, M. Sakai, Y.S. Meng, Nat. Commun. 7 (2016) 1-8.
- [19] T. Liu, X. Wei, Z. Nie, V. Sprenkle, W. Wang, Adv. Energy Mater. 6 (2016) 1501449.
- [20] C. DeBruler, B. Hu, J. Moss, J. Luo, T.L. Liu, ACS Energy Lett. 3 (2018) 663–668.
- [21] T. Janoschka, N. Martin, U. Martin, C. Friebe, S. Morgenstern, H. Hiller, M.D. Hager, U.S. Schubert, Nature 527 (2015) 78-81.
- [22] K. Peng, P. Sun, Z. Yang, T. Xu, Batter. Supercaps., e202200426.
- [23] Y. Liu, Y. Li, P. Zuo, Q. Chen, G. Tang, P. Sun, Z. Yang, T. Xu, ChemSusChem 13 (2020) 2245-2249.
- [24] M. Hu, W. Wu, J. Luo, T.L. Liu, Adv. Energy Mater. 12 (2022) 2202085.
- [25] A. Hollas, X. Wei, V. Murugesan, Z. Nie, B. Li, D. Reed, J. Liu, V. Sprenkle, W. Wang, Nat. Energy 3 (2018) 508–514.
- [26] S. Pang, X. Wang, P. Wang, Y. Ji, Angew. Chem. Int. Ed. 133 (2021) 5349-5358.
- [27] J. Xu, S. Pang, X. Wang, P. Wang, Y. Ji, Joule 5 (2021) 2437-2449.
- [28] R. Feng, X. Zhang, V. Murugesan, A. Holias, Y. Chen, Y. Shao, E. Walter, N.P.N. Wellala, L. Yan, K.M. Rosso, W. Wang, Science 372 (2021) 836-840.
- [29] E.S. Beh, D. De Porcellinis, R.L. Gracia, K.T. Xia, R.G. Gordon, M.J. Aziz, ACS Energy Lett. 2 (2017) 639-644.
- [30] B. Hu, C. DeBruler, Z. Rhodes, T.L. Liu, J. Am. Chem. Soc. 139 (2017) 1207–1214.
- [31] J. Luo, B. Hu, M. Hu, W. Wu, T.L. Liu, Angew. Chem. Int. Ed. 61 (2022) e202204030.
- Y. Liu, M.-A. Goulet, L. Tong, Y. Liu, Y. Ji, L. Wu, R.G. Gordon, M.J. Aziz, Z. Yang, T. Xu, Chem 5 (2019) 1861-1870.
- [33] H. Fan, W. Wu, M. Ravivarma, H. Li, B. Hu, J. Lei, Y. Feng, X. Sun, J. Song, T.L. Liu, Adv. Funct. Mater. 32 (2022) 2203032.
- C. Zhang, Z. Niu, S. Peng, Y. Ding, L. Zhang, X. Guo, Y. Zhao, G. Yu, Adv. Mater. 31 (2019) 1901052
- [35] J. Zhang, I.A. Shkrob, R.S. Assary, So Tung, B. Silcox, L.A. Curtiss, L. Thompson, L. Zhang, J. Phys. Chem. C 121 (2017) 23347-23358.
- [36] S.M. Oliveira, M.A. Segundo, A.O. Rangel, J.L. Lima, V. Cerda, Anal. Lett. 44 (2011) 284-297
- [37] S. Katsamakas, A.L. Zografos, V. Sarli, Curr. Med. Chem. 23 (2016) 2972-2999.
- [38] F. Otteny, V. Perner, D. Wassy, M. Kolek, P. Bieker, M. Winter, B. Esser, ACS Sustain. Chem. Eng. 8 (2019) 238-247.
- [39] K. Lee, I.E. Serdiuk, G. Kwon, D.J. Min, K. Kang, S.Y. Park, J.E. Kwon, Energy Environ. Sci. 13 (2020) 4142-4156.
- [40] Y. Yan, R. Walser-Kuntz, M.S. Sanford, ACS Mater. Lett. 4 (2022) 733-739.
- H. Li, H. Fan, M. Ravivarma, B. Hu, Y. Feng, J. Song, Chem. Commun. 56 (2020) 13824-13827.
- [42] R.S. Nicholson, I. Shain, Anal. Chem. 36 (1964) 706-723.
- [43] M. Gao, M. Salla, Y. Song, Q. Wang, Angew. Chem. Int. Ed. 61 (2022) e202204030.
- [44] J. Luo, B. Hu, M. Hu, W.D. Wu, T.L. Liu, Angew. Chem. Int. Ed. 61 (2022) e202208223.
- [45] C. DeBruler, B. Hu, J. Moss, X. Liu, J. Luo, Y. Sun, T.L. Liu, Chem 3 (2017) 961–978.
- [46] A.Z. Weber, M.M. Mench, J.P. Meyers, P.N. Ross, J.T. Gostick, Q. Liu, J. Appl. Electrochem. 41 (2011) 1137-1164.
- [47] J. Luo, B. Hu, M. Hu, Y. Zhao, T.L. Liu, ACS Energy Lett. 4 (2019) 2220-2240.
- [48] P. Zuo, J. Zhou, Z. Yang, T. Xu, ChemPlusChem 85 (2020) 1893-1904.
- [49] J. Xu, S. Pang, X. Wang, P. Wang, Y. Ji, Joule 5 (2021) 2437-2449.
- [50] M. Wu, Y. Jing, A.A. Wong, E.M. Fell, S. Jin, Z. Tang, R.G. Gordon, M.J. Aziz, Chem 6 (2020) 1432-1442.
- [51] S.-M. Wu, The Chemistry of 10-Phenylphenoxazine Cation Radical Perchlorate, Texas Tech University, 1977.
- D. Sun, S.V. Rosokha, J.K. Kochi, J. Am. Chem. Soc. 126 (2004) 1388–1401.
- S. Suzuki, R. Maya, Y. Uchida, T. Naota, ACS Omega 4 (2019) 10031-10035.
- [54] I.A. Shkrob, L.A. Robertson, Z. Yu, R.S. Assary, L. Cheng, L. Zhang, E. Sarnello, X. Liu, T. Li, A.P. Kaur, J. Mol. Liq. 334 (2021) 116533.